Journal of Environmental Chemical Engineering 10 (2022) 107670

Contents lists available at ScienceDirect

Journal of Environmental Chemical Engineering

journal homepage: www.elsevier.com/locate/jece

Coupled electrochemical transformation and filtration of water pollutants by cathodic-carbon nanotube membranes

Chidambaram Thamaraiselvan [a,1], Woei Jye Lau [b], Carlos G. Dosoretz [a,*]

[a] Faculty of Civil and Environmental Engineering, Technion-Israel Institute of Technology, Haifa 3200003, Israel
[b] Advanced Membrane Technology Research Centre, Universiti Teknologi Malaysia, 81310 Skudai, Johor, Malaysia

ARTICLE INFO

Editor: Dong-Yeun Koh

Keywords:
Support free CNT membranes
Electrochemical reduction
Resazurin
Diatrizoate
Hexavalent chromium

ABSTRACT

This study aimed at evaluating the concomitant electrochemical reduction and separation of organic and inorganic model contaminants from water. A highly conductive (40,000 S/m) support free carbon nanotube (CNT) membrane was used as a cathode in a three-electrode electrochemical crossflow membrane filtration system. Diatrizoate (DTZ), a recalcitrant iodinated contrast media; resazurin (RZ), a redox indicator; and hexavalent chromium ion (Cr(VI)), a 'gold' standard for characterization of reducing systems, were tested as model contaminants. Voltages of −0.6 to −1.0 V were enough to remove between 90% and 95% of the three model contaminants tested. Removal of Cr(VI) proceeded by reduction to Cr(III) followed by adsorption onto the cathode, which could be efficiently regenerated (up to 95%) applying reversal (anodic) potential. Preliminary findings applying AC current (0.6–1.5 V, 10 Hz-1 kHz) suggest that it could be a feasible approach for detoxification with minimization of membrane clogging. Resazurin was immediately transformed into resorufin to near completion which was in turn further reduced to dihydroresorufin. The reductive transformation of DTZ resulted in almost complete deiodination, leading to the accumulation of 3,5-diacetamidobenzoic acid as the main end-product. Although other five secondary transformation products were detected, four of them were fully deiodinated. Concluding, the proposed electrochemical filtration cell equipped with a highly conductive CNT-cathodic membrane can be regarded as a potential technique for water decontamination and effective dehalogenation of organic compounds.

1. Introduction

Electrochemical processes have attracted great attention in recent years for water and wastewater detoxification due to their efficiency over typical treatments [1]. These techniques provide adaptable and cost-effective treatment solutions for heavy metals and micropollutants removal, offering an alternative key to many environmental and industrial problems. Carbon nanotubes (CNTs), similarly to other conductive carbon nanomaterials, have a wide potential in water and wastewater treatment and decontamination applications due to their inherent antibacterial characteristics, physical and chemical properties, and high electrical conductivity [2–4]. In addition to fouling-resistant systems for desalination, they display enhanced solute separation, and innovative electrocatalytic platforms for pollutants removal. Over the past few decades, the cost-effective CNT-based electrocatalysts have been studied to remove pollutants due to their unique structural and electrical properties [5,6].

Many literature reports are available on water and wastewater treatment using electroconductive CNT based membranes, most if not all performed in batch mode. For example, an electrochemically active filter made of multiwalled carbon nanotube (MWCNT) filter was studied for the adsorptive removal and electrochemical oxidation of the aqueous dyes (methylene blue and methyl orange) and aqueous anions (chloride and iodide) [7]. This study was done in dead-end filtration mode at a low flow rate of 1.5 ± 0.1 mL/min. Simultaneous dechlorinationation and oxidation of organic compounds during filtration through a cathodic CNT membrane was reported. Reactive oxidant species were generated by the reductive decomposition of chlorine through the catalytic interaction with CNT [8]. Electrochemical oxidation with a CNT filter was also studied for removal and inactivation of viruses [9] and bacteria [3,5]. In addition, improved electrosorption efficiency was observed with CNT-chitosan composites [10]. Stainless steel nets coated with single

* Corresponding author.
E-mail address: carlosd@technion.ac.il (C.G. Dosoretz).
[1] Present address: Interdisciplinary Centre for Energy Research, Indian Institute of Science, Bengaluru 560012, India.

https://doi.org/10.1016/j.jece.2022.107670
Received 30 November 2021; Received in revised form 18 March 2022; Accepted 4 April 2022
Available online 8 April 2022

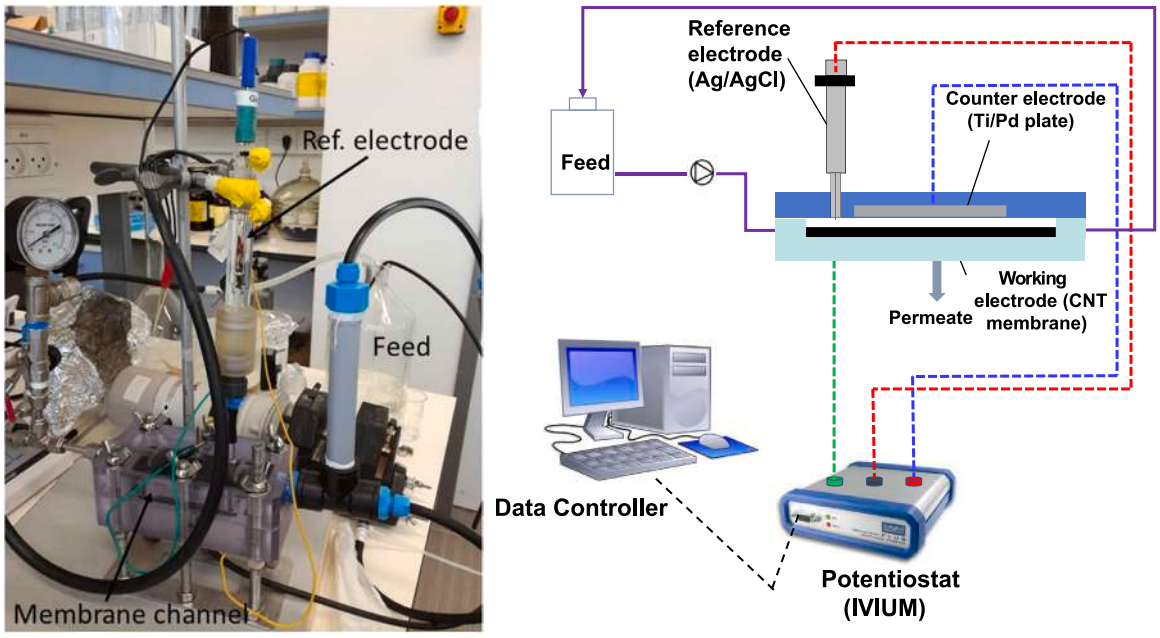

Fig. 1. Setup of the experimental flow-through electrochemical reduction system. Left: Photograph of the crossflow membrane cell, with pumps, gauges and electrodes. Right: Schematic diagram of the whole electrochemical flow-through system. WE-Working electrode/cathode (CNT membrane), CE-Counter electrode/anode (Ti/Pd), RE-Reference electrode (Ag/AgCl).

wall carbon nanotubes (SWCNT) were used for electrochemical removal of chromium and lead in batch mode [11,12]. Moreover, catalyst doped CNT electrodes were demonstrated for different kinds of pollutants removal in batch mode studies. For instance, manganese oxide MnO_2/MWCNT hybrids were used for tetrabromobisphenol A degradation [13] and Pt, Pd, Ru-Cu supported-CNT electrode was studied for aniline oxidation [14].

Some other electro-reactive membranes have been reported for degradation for different pollutants, with emphasis on pharmaceutical active compounds. For example, Misal et al. [15] used a porous Ti_4O_7 and Pd-Cu doped Ti_4O_7 reactive membrane to study electrochemical oxidation and reduction of sulfamethoxazole. Embedded nano zero-valent iron (nZVI) particles into single and double-walled carbon nanotubes were studied as a mean for the regeneration of the electro-conductive membrane surface as well as enhanced electrochemical oxidation of pollutants in continuous regime, such azo dyes [16] and metropolol [17]. Highly electrically conductive CNTs enable the direct transfer of electrons to the metallic nanoparticles, however, keeping an inert atmosphere is a critical challenge during the fabrication of nZVI embedded-CNT membranes [17]. Zhao et al. [18] studied the electrochemical oxidation of bisphenol A during flow-through filtration through an anodic CNT membrane coated with bismuth-doped tin dioxide. Similarly, TiO_2 porous nanotube arrays plates modified with NH_4F and $(NH_4)_2SO_4$ were used as anodic membrane for carbamazepine [19] and triclosan [20] electrochemical oxidation in flow-through in full-recirculation mode. In most if not all cases, flow through transformation was performed in ultra-low flow rate to enhance the reaction time. This, in addition to the mass of the electro-reactive membranes, seems imperative to allow sufficient reaction time for transformation during filtration [8].

In previous works, we thoroughly characterized the application of CNT laminates as support free-membranes owning very high electrical conductivity (≥40,000 S/m), and successfully demonstrated the effect of the electrical field for potential biofouling prevention [3,21]. Herein we present the application of these CNT laminates as a cathode in a cross-flow electrochemical setup mimicking a spiral wound membrane filtration system at a linear velocity of ~0.15 m/s, to reduce and remove water pollutants in continuous regime. For this purpose, three model contaminants were selected: diatrizoate (DTZ), a iodinated contrast media (ICM), resazurin (RZ), a redox indicator, and hexavalent chromium (Cr(VI)) ion, a 'gold' standard for characterization of reducing systems. Typically, Cr(VI) could be found in the industrial processes dealing with dyeing, electroplating, metal finishing, and tanning [15]. Resazurin, is widely used for cell viability and aerobic microbial activity assays as well as in a clinical research for the determination of antibacterial activity, including susceptibility of pathogens [22]. RZ is a phenoxazin-3-one dye with nitrone functional group that can be irreversibly reduced to resorufin (RF) which can be further reversibly reduced to dihydro-resorufin, providing color changes from purple to pink and ultimately to colorless [23]. Because of its established reduction pattern and simplicity of tracking, resazurin was added as an organic model compound for qualitative and quantitative characterization of cathodic reduction.

ICMs owning a characteristic substituted triiodobenzene ring are typical contaminants frequently detected in municipal wastewater treatment at relatively high concentrations at peak activity of medical centers, *i.e.*, up to 0.2–10 μg/L median concentration [24,25]. Interestingly, DTZ which is among the most difficult to oxidize ICMs, has been reported among the most persistent ICMs with respect to reduction [26]. Thus, it is a good indicator for assessing the efficacy of reductive treatment. Electrochemical reduction of highly substituted halogenated compounds has received growing attention, due to its efficiency, easy automatization, versatility, and environmental compatibility [27]. However, detailed information on the mechanism of electrochemical dehalogenation of ICM is very limited. To evaluate and characterize the potential of simultaneous reduction and filtration of these model pollutants during water treatment, a three electrode-electrochemical membrane filtration setup comprising a palladium coated-titanium anode, a CNT-membrane cathode and a reference electrode, was applied. Orbitrap liquid chromatography-mass spectrometry (LC-MS) was employed to analyze DTZ transformation in depth.

2. Materials and methods

2.1. Chemicals

All chemical used for the experiments were at least of analytical grade. Diatrizoate and resazurin were purchased from Sigma-Aldrich. CNT membrane used in this work was obtained from Tortec Nano Fibers [21].

2.2. Experimental set-up

The electrochemical reduction experiments were performed in a flow-through electrochemical system comprising a single channel crossflow membrane filtration cell holding three electrodes. The support free-CNT membrane was used as a cathode (working electrode), and a palladium coated-titanium anode was used as a counter electrode. A 3 M Ag/AgCl reference electrode was placed very close to the working electrode (about 3 mm distance), and the current was recorded every 60 s. All currents/potentials were measured against the built-in reference electrode (+0.210 V *vs*. Ag/AgCl). Reduction experiments were conducted potentiostatically at cathode potentials ranging from −1.6 to −1.2 V *vs*. Ag/AgCl using an IVIUM potentiostat/galvanostat (Vertex10A). A view and schematic setup diagram of the flow-through electrochemical system is presented in Fig. 1.

Experiments were performed in either non-filtration mode (no pressure applied throughout the membrane) or filtration mode (transmembrane pressure applied), as indicated. Regarding filtration experiments, unless otherwise indicated, they were conducted in full batch mode (both retentate and permeate were recirculated back to the feed tank).

A detailed description of the filtration cell setup was published elsewhere [3]. This cell was equipped with pressure gauges and pressure transducers (inlet and outlet pressure), and flow-valve controller and operated at a low linear flow velocity of ~0.15 m/s and 10 psi inlet pressure. The effective surface area of the membrane was 24 cm^2. Regardless of the operation mode, prior to experiments, the membranes were soaked overnight in distilled water and assembled in the cleaned flow cells, washed with filter-sterilized distilled water for 1 h and then equilibrated with the feed solution. All solutions were flushed with nitrogen gas for 30 min prior to use, while during the experiments, the system was deoxygenated by sparging nitrogen gas in the cathodic recirculation stream.

All experiments were performed using a 100 mM sodium sulfate ($NaSO_4$) solution in ultrapure water as background electrolyte. As indicated, the model compounds were spiked into the feed tank to a final concentration of 2 mg/L for Cr(VI) or 10 mg/L for DTZ and RZ. At the end of the experiments, the membrane was thoroughly flushed with ultrapure water and taken for microscopy observation.

For experiments performed in filtration mode, the membrane productivity was expressed as relative permeability, as defined in Eq. (1):

$$\text{Relative permeability} = \frac{Lp_t}{Lp_o} \tag{1}$$

whereas Lp is the permeability through the membrane in L/m^2.h.bar units (LMH/bar), as defined in Eq. (2), at initial time before electrical current was applied (Lp_o) and t-time (Lp_t):

$$Lp = \frac{V_w}{A \times t \times p} = \frac{J_w}{p} \tag{2}$$

In which V_w, A, t and p are the volume of permeate (L), area of the membrane (m^2), permeate collection time (h) and inlet pressure (bar), respectively and J_w is the permeate flux (LMH).

The removal of a model pollutant was defined as follows:

I. The bulk removal, representing the relative overall change in concentration in the system measured in the feed tank, was calculated as defined in Eq. (3):

$$\text{Bulk removal } (\%) = \left(1 - \frac{Cb_t}{Cb_o}\right) \times 100 \tag{3}$$

where Cb_o and Cb_t are the initial and t-time concentration of the model pollutant in the bulk solution, comprising the recycled retentate and permeate blended back in the feed tank in full batch mode or just the recycled retentate blended in the feed tank in permeate release mode.

II. Membrane removal, indicating the relative change in concentration throughout the membrane, was calculated as defined in Eq. (4):

$$\text{Membrane removal } (\%) = \left(1 - \frac{Cp_t}{Cb_o}\right) \times 100 \tag{4}$$

where Cp_t is t-time concentration of the model pollutant in the permeate.

2.3. Electrochemical characterization

The relative potential of the membrane *vs*. Ag/AgCl reference electrode was determined as a function of the applied cell potential by placing the CNT membrane (cathode), a pristine palladium-coated titanium sheet (anode) and a reference electrode in a glass beaker containing electrolyte solution (Na_2SO_4). The cell potential was applied to the membrane and titanium counter electrode using a DC power source, and the relative potential on the membrane was determined by connecting the membrane, counter electrode and reference electrode to a potentiostat, which measured the open-circuit potential on the membrane (working electrode) in 2 mg/L Cr(VI) solution. Though acidic pH favors Cr(VI) removal, the pH of the solution was kept at 7 to mimic real water treatment conditions and avoid pH control, which is an additional and costly operation in full-scale processes.

The electrochemical behavior of cathodic Cr(VI), DTZ and RZ reduction were investigated by background subtracted-cyclic voltammetry (CV). Experiments were performed using a 2 mg/L Cr(VI), 10 mg/L RZ and 10 mg/L DTZ solution at pH 7 with 100 mM Na_2SO_4 as the supporting electrolyte. All solutions were purged with nitrogen for 30 min prior to use. Background CV experiments were conducted under identical conditions, except that the model compounds (Cr(VI), RZ and DTZ) were omitted. Then, the background CV curves were subtracted from the CV curves generated in the presence of pollutants. In all CV experiments, the scan rate was held at 50 mV/s with the voltage ranging between 1 and −1.5 V.

2.4. Analytical techniques

Thorough surface characterization of the membrane was performed by scanning electron microscope (SEM), energy dispersive X-ray spectroscopy (EDS) and X-ray photoelectron spectroscopy (XPS). High resolution (HR)-SEM was conducted in a Carl Zeiss Ultra-Plus FE-SEM and EDS (FEI E-SEM Quanta 200). Prior to imaging, samples were sputter coated with carbon.

Surface analysis of the CNT membranes was performed on a Versaprobe III-PHI Instrument (Physical Electronics) with a Al Kα at 1486.6 eV monochromatic source (X-ray beam size 200 μm, 25 W, 15 kV) and a spherical electron energy analyzer [21]. To determine chemical functionalities at elements environment a High-Resolution X-ray Photoelectron Spectroscopy (HR-XPS) was measured for the samples (Pass Energy = 55 eV and a step size of 0.05 eV). The core level binding energies of the different peaks were normalized by setting the binding energy for the C1s at 284.5 eV. The crystallographic information of the CNT membrane was investigated by X-ray diffraction (XRD) (Shimadzu X-ray diffractometer 6000, Cu Kα radiation, Kyoto, Japan) with a scan rate of 1°/min.

DTZ was quantified by LC-MS on a Agilent 1200 HPLC (Hewellet Packard) coupled with ion spray interface to a triple quadrupole mass spectrometer (API 3200, Applied Biosystems), as detailed by Azerrad

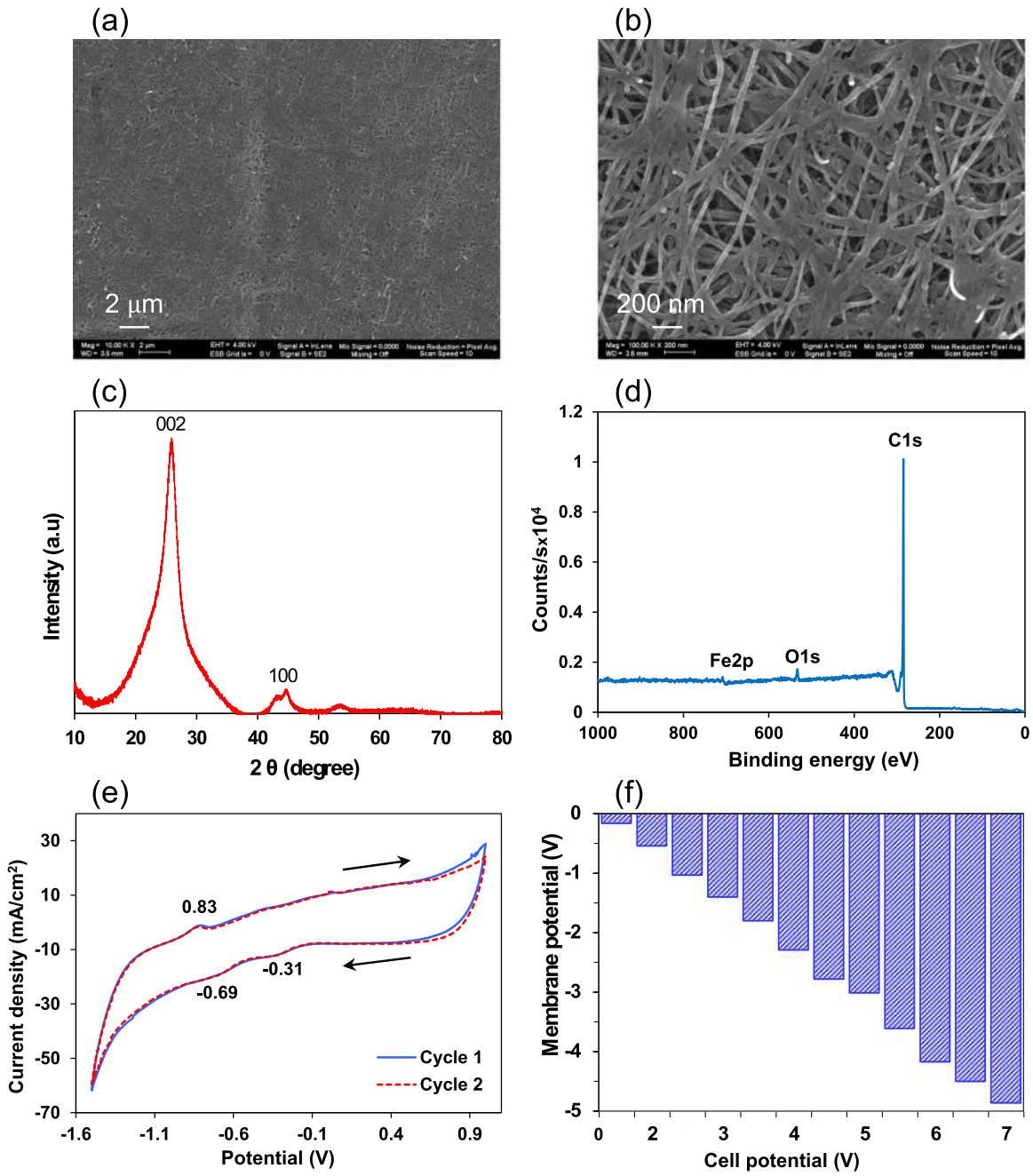

Fig. 2. Relevant properties of the support free-CNT membrane used in this study. (a,b) HR-SEM surface morphology at magnification of 10 and 100 K, respectively; (c) XRD spectrum; (d) XPS spectrum; (e) cyclic voltammogram of the 2 mg/L Cr(VI) solution using CNT membrane as a working electrode at a scan rate of 50 mV/s *vs.* Ag/AgCl reference electrode (2 cycles); (f) cathodic potential on the membrane at different cell potentials.

et al. [28]. Electrospray ionization was used in a positive ion mode and quantification was performed in multiple-reaction monitoring (MRM) mode. Chromatography separation was performed on a C18 reverse-phase column (Purospher, Merck) with 0.1% formic acid in DDW and methanol as eluent.

DTZ transformation products were analyzed by LC-MS on a Dionex Ultimate 3000 RS HPLC coupled to a Q Extractive Plus hybrid FT mass spectrometer equipped with heated electrospray ionization source (Thermo Fisher Scientific Inc.). Chromatographic separation of compounds was carried out using Acclaim C18 column (150 ×2.1 mm, 2.2 µm, Thermo Scientific) and data were analyzed using Xcalibur software (Thermo Fisher Scientific). Mass spectrometer was operated in positive and negative ESI modes, ion source parameters were as follows: spray voltage 3 kV, capillary temperature 300 ℃, sheath gas rate (arb) 40, and auxiliary gas rate (arb) 10. Mass spectra were acquired in scan mode; resolving power was 70.000).

Iodide release was quantified by ion conductivity chromatography on a 881 Compact IC Pro with chemical suppression (Metrohm), equipped with a 4 µm pore size IC-SI-52 4E column (Shodex) and sodium carbonate as eluent [29]. The limit of detection of iodide ion analysis is 30 µg/L.

Dissolved organic carbon (DOC) was measured on a total organic carbon (TOC) analyzer (TOC-VCPH, Shimadzu) following acidification; inorganic carbon (IC) was calculated from total carbon determined prior to acidification [29]. Cr(VI) concentrations were measured by a colorimetric method using diphenyl-carbazide as a complexing agent [30,31]

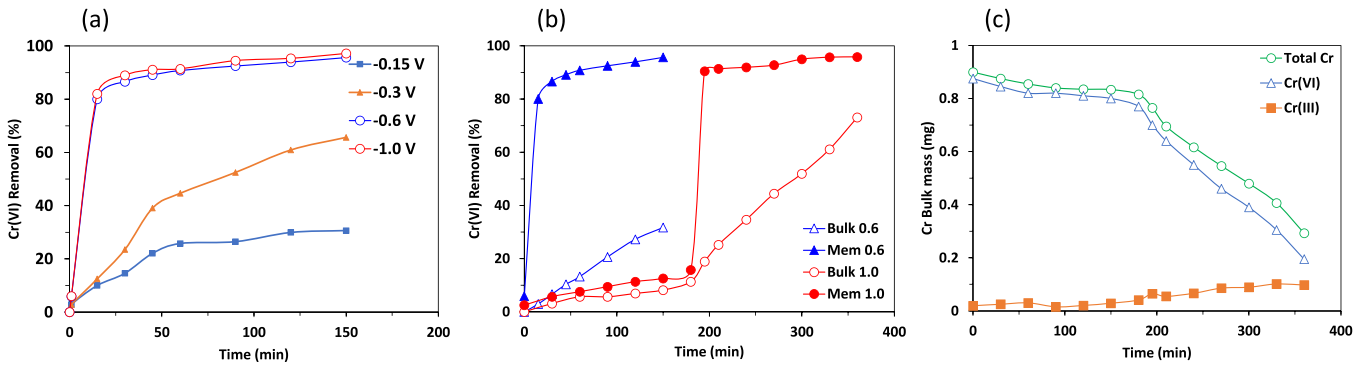

Fig. 3. Characterization of hexavalent chromium removal (2 mg/L) in the flow-through electrochemical system with a cathodic CNT membrane and a palladium coated-titanium anode against an Ag/AgCl reference electrode. (a): Effect of different electric potentials applied in non-filtration mode on Cr(VI) removal; (b): Cr(VI) removal profiles in filtration mode at applied potential of −0.6 V and −1.0 V. For this last potential, electricity was started after 180 min; (c): Mass balance profile of dissolved chromium species in filtration mode at −1.0 V in the bulk solution, comprising the recycled retentate and permeate blended back into the feed. Bulk removal represents the overall change in Cr(VI) in the system (see Eq. (3)). Membrane (Mem) removal represents the change in Cr(VI) throughout the membrane (see Eq. (4)).

followed by measuring light absorption at 540 nm using a UV–visible spectrophotometer (Agilent 8453 series). Total chromium was measured using inductively coupled plasma-atomic emission spectrometer (iCAP-6300, Thermo Sci). Cr(III) concentrations were calculated by subtracting Cr(VI) from the total chromium concentration. RZ and its transformation product RF were monitored by scanning UV/visible spectrophotometry (Agilent 8453 series).

3. Results and discussion

3.1. Characterization of the support free-CNT membrane

The key properties of the support free-CNT membrane that are most relevant for this study are presented in Fig. 2. These membranes are characterized by dense fibers entangled multi-directionally which enhances the membrane performance in multidirectional/multiple ways such as rejection, electrical conductivity, and flux, as depicted by the typical HR-SEM micrographs shown in Fig. 2. Full details on the morphology of CNT membrane are detailed in our previous work [21]. With respect to the XRD pattern, the presence of two peaks at 26.14° and 44.22° in the CNT membrane (Fig. 2c), corresponding to an interplanar space of 3.41 Å and 2.05 Å, respectively, which can be correspondingly indexed as 002 and 100 reflections of graphite [32]. The XPS spectrum as presented in Fig. 2d meanwhile shows that besides carbon and oxygen, there were also trace amount of iron (~1%) detected on the membrane. The existence of such an element is due to the use of catalysts during CNT laminate synthesis.

Fig. 2e shows a typical cyclic voltammogram obtained when a CNT membrane was placed as a cathodic electrode against a Ti/Pd counter electrode, *vs.* an Ag/AgCl reference electrode, within an electrochemical circuit in contact with 2 mg/L Cr(VI) solution in the presence of a Na_2SO_4 electrolyte solution. When chromium was present in the solution, a typical cyclic voltammogram depicted a cathodic current with two reduction peaks at −0.31 V and −0.66 V (*vs.* Ag/AgCl). These peaks were not sharp enough compared to standard CV analysis, due to the overall intrinsic resistance of the system as a function of electrolyte concentration, large electrode size and cleanliness, and aqueous phase volume. These reduction potentials are in line with the characteristic of the reduction potential of CrO_4^{2-} (−0.6 V) when graphitic carbon electrodes were used [30] and the reduction potential of $HCrO_4^-$ (−0.3 V) when glassy carbon was used as electrode [33].

The variation of the cell potential *vs.* the Ag/AgCl reference had an immediate impact on the relative potential of the membrane (Fig. 2f). Indeed, upon application of the cell potential, there was an initial decrease in the cathodic potential of the membrane, which reached a stable value after approximately 1 min. This behavior is in line with the corrosion of a titanium counter electrode when it was exposed to anodic-oxidizing currents [30]. Since the support free-CNT membrane used in this study owns extremely high conductivity (> 40,000 S/m) [14], the membrane potential remained very high; for instance, −4.9 V of membrane potential was attained for 7 V cell potential. These values are significantly higher than the CNT composite conductive membranes reported in the literature [2]. The higher the membrane potential is likely to improve the efficiency of the electrochemical removal/reduction of pollutants. Furthermore, because the whole membrane applied in this research is conductive, an increase in the contact surface area is expected that in turn would enhance the kinetics of the reduction reaction, in line with previous reports, as summarized by Peng and Guo [34].

3.2. Hexavalent chromium reduction

As the Cr(VI) model solution was prepared from $K_2Cr_2O_7$, the three main expected anionic species in solution are $Cr_2O_7^{2-}$, CrO_4^{2-} and $HCrO_4^-$, at different proportions depending on the pH [34]. Convection, electromigration and diffusion forces induce the displacement of ions towards and at the electrode surfaces in electrochemical systems [35, 36]. When operating the electrochemical system under an electricity field in the range of 0 to –1 V, transfer of electrons from a cathode to the Cr(VI) ions would reduce it to Cr(III) ions. The main possible cathodic reactions as a function of the pH [30,37,38] are as follows:

$$2H^+ + 2e^- \rightarrow H_{2(g)}; \quad E^\circ = 0\ V \tag{5}$$

$$5H^+_{aq} + CrO^{2-}_{4(aq)} + 3e^- \rightarrow Cr(0H)_{3(s)} + H_2O; \quad E^\circ = -0.13\ V \tag{6}$$

$$Cr(OH)_{3(s)} + e^- \rightarrow Cr(OH)_2 + OH^-; \quad E^\circ = -1.1\ V \tag{7}$$

The impact of the concentration of the background electrolyte (Na_2SO_4) on Cr(VI) reduction was first evaluated in the range of 0 mM (DI water) to 200 mM at −1 V applied potential. The Cr(VI) reduction rate increased proportionally up to 100 mM and then remained steady (Fig. S1). Because of this, 100 mM was used as the concentration of background electrolyte for all further experiments. Cr(VI) reduction was then studied under non-filtration and filtration conditions (Fig. 3). The effect of the variation of the relative potential applied on Cr(VI) reduction in non-filtration mode was characterized in the range of −0.15 to −1.0 V (Fig. 3a). Cr(VI) reduction efficiency increased with the increase of the relative voltage applied, most likely due to the augmentation of the electrostatic attraction, reaching a maximum (>95%) at voltage values of ≥ −0.6 V, in line with the characteristic

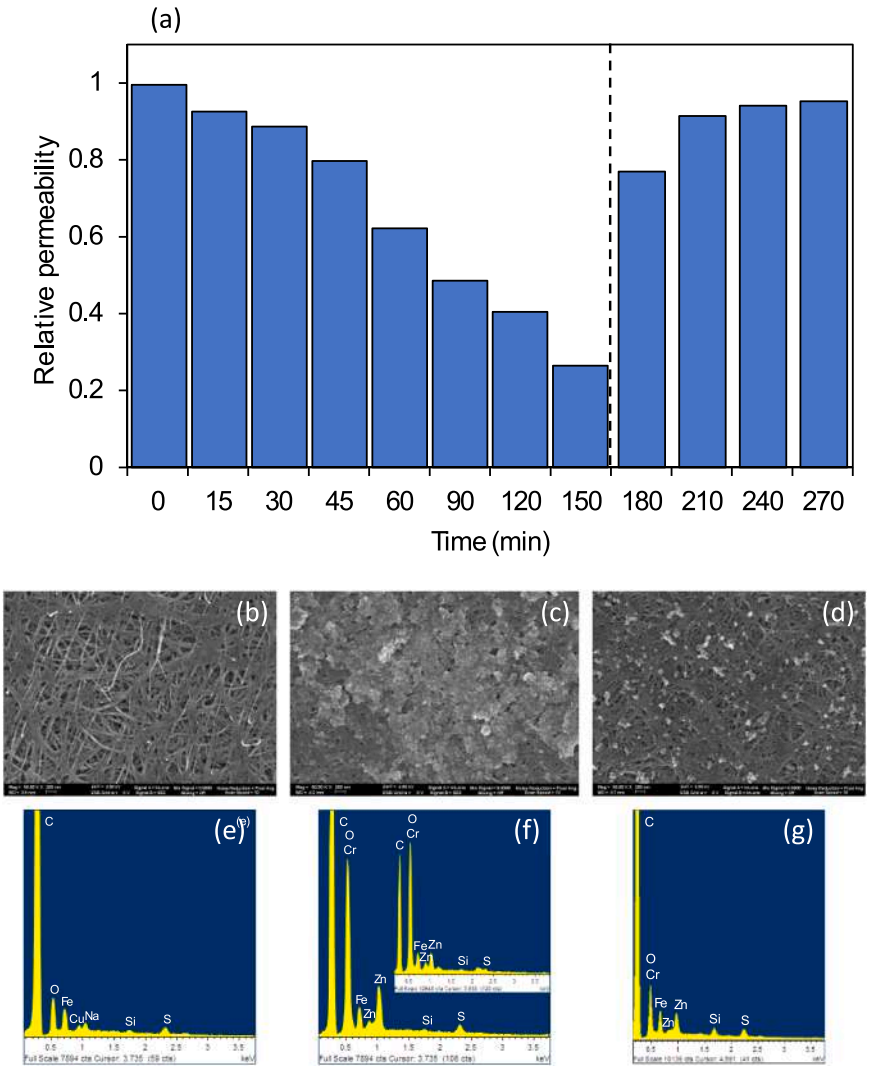

Fig. 4. Characterization of the CNT membrane performance with cathodic current (reduction) and after membrane regeneration with anodic current (desorption). Relative permeability (a). SEM micrographs: (b) virgin; (c) cathodic potential; (d) anodic potential. EDS profiles: (e) virgin; (f) cathodic potential (Inset shows a profile of a thick deposition zone); (g) anodic potential. Applied current was at −1 V potential. The relative permeability was normalized to the initial value before (215 ± 10 LMH/bar) electrical current was applied (see Eq. (1)).

reduction peak at −0.69 V found by CV (see Fig. 2e above).

Then, Cr(VI) reduction and removal were tested in filtration mode, at both −0.6 V and −1.0 V (Fig. 3b) applied potential. As can be seen from the data presented, 85–95% of the Cr (VI) removal was achieved in the permeate regardless of the potential applied, whereas 10–30% and 10–50% removal was attained in the bulk solution of −0.6 and −1.0 V, respectively. Because of the consumption of hydrogen ions in the reduction reactions, the pH of the permeate increased from ~6.2 to above neutrality during the 2.5 h operation, whereas the bulk pH remained practically steady. The mass balance of chromium ions in the electrochemical system at −1 V, comprising reduction and filtration, depicts an overall transformation of approx. 68% (Fig. 3c). The time profiles of the bulk and permeate streams before electricity was applied, *i.e.*, before reduction started, point out minimal Cr(VI) adsorption onto the membrane. Upon reduction, a low mass of Cr(III) ions in solution could be detected, indicating that 84% Cr(III) generated upon Cr(VI) reduction, in turn, deposited onto the surface of the cathodic membrane. Moreover, the kinetics of hexavalent chromium reduction studied at −1 V for 2 h at different concentrations in the range of 1–8 mg/L followed a pseudo first-order kinetics, with a rate constant of 0.11 ± 0.02 mg/L.min). All together, these results indicate that Cr(VI) reduction rate was not substantially affected by Cr(III) adsorption due to the high surface area of the porous membrane/cathode, in line with Wang and Na [39].

The impact of the deposition of chromium on the cathodic membrane during electrochemical reduction was further characterized (Figs. 4 and 5, Table 1). Although the normalized flux through the membrane decreased by 70% in 150 min when the cathodic current was applied (Fig. 4a), it could be regenerated up to almost 95% of the initial flux by reversal potential (anodic current). As a consequence of the detachment of the foulants from the membrane by inverting the electrical potential, which can be applied as a kind of clean-in-place procedure, an average relative flux of 0.75 could be maintained throughout the filtration process without the need for chemical cleaning.

The effect of Cr(VI) reduction and separation, on the morphology of the membrane visualized by SEM, as well as that of the electrochemical desorption, are shown in Fig. 4b-d. When the reduction process occurs, it is likely to reduce and deposit as Cr(III) complex on the cathode as are comparatively shown in Fig. 4b,c. The adsorption of chromium ions on the membrane surface during filtration upon hexavalent chromium reduction, creating evident deposition spots as depicted by the SEM micrographs, were further confirmed by EDS analysis (Fig. 4e,f).

Similarly, when the anodic potential was applied to the CNT membrane, substantial removal of the Cr(III) deposited could be attained, as can be seen from the SEM micrograph (Fig. 4d) and relative peak intensity in the EDS profile in Fig. 4g. The recovery of the performance of the CNT membranes upon regeneration was reconfirmed in new reduction experiments (data not shown).

The surface of the CNT membranes was also examined by high-resolution XPS to further characterize chromium adsorption and

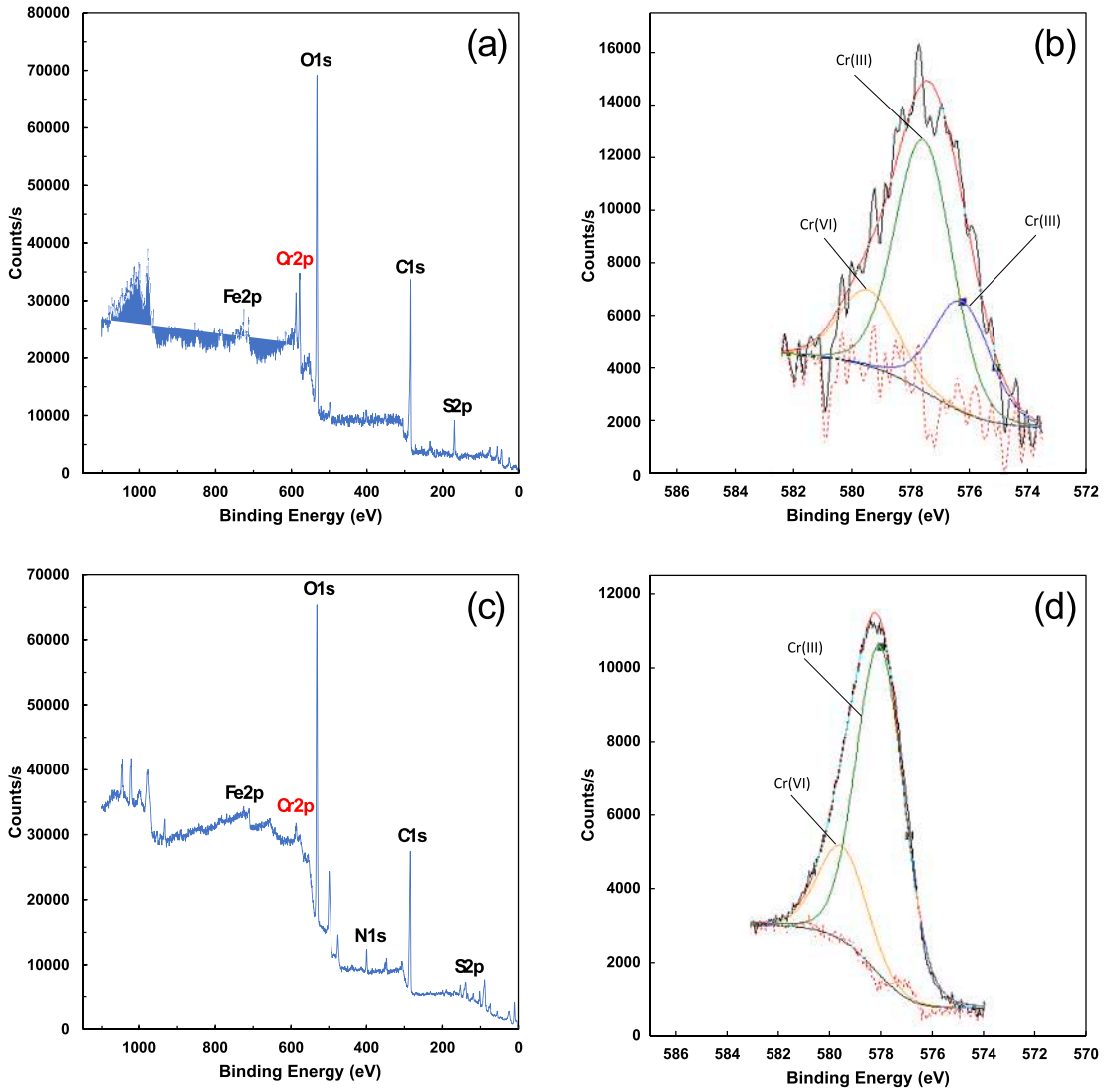

Fig. 5. XPS analysis of the CNT membranes studied for Cr removal. Cathodic potential: (a) XPS survey scan; (b) High-resolution XPS of chromium deconvolution. Anodic potential: (c) XPS survey scan; (d) High-resolution XPS of chromium deconvolution. Applied potential was −1 V. Survey scan of the membranes was performed after 150 min of cathodic potential. For the survey scan of the virgin membrane, refer to Fig. 2d.

Table 1
Elemental XPS-surface composition (in %).

Sample	O1s	C1s	Fe2p3	Cr2p3	N1s	S2p
Virgin	2.9	95.9	0.8	–	–	0
Cathodic	41.4	48.0	1.4	4.3	1.0	2.8
Anodic	40.2	47.8	0.6	0.5	1.8	0.2

desorption during the electrochemical-filtration cycle. The elemental composition of virgin, cathodic and anodic potential applied membranes is shown in Table 1. As can be seen, about 4.3% chromium accumulated on the surface, and around 0.5% remained in the membrane upon desorption with anodic current, whereas chromium was absent in the control. The XPS spectra are presented in Fig. 5. The broad spectrum-survey of the membranes with either cathodic or anodic potentials applied are shown in Fig. 5a and c, respectively, depicting the presence of a Cr2p peak. The high resolution-spectrum of Cr2p (Fig. 5b, d) includes the Cr2p2/3 (578 eV) envelope. The deconvolution lines confirm two kinds of chromium species on the membrane surface, Cr(III) and Cr (VI). For the cathodic potential (reduction) (Fig. 5b), the primary peak suggests that the dominant species present on the membrane was in the form of Cr(III) as a complex of Cr_2O_3 and $Cr(OH)_3$ subspecies, with corresponding peaks at 576.5 eV [31] and 577.8 [31]. Cr(VI) might also be slightly adsorbed on the membrane as depicted by the weak peak at 579.6 eV, most probably in the form of $(Cr_2O_7)^{2-}$. Thus, it can be concluded that the main species of chromium that was deposited on the membrane surface were Cr(III), most probably following the stoichiometry presented in Eq. (6) at the pH of the reaction, in agreement with the findings of Yao et al. [40]. For the regeneration step (anodic current), presenting a lower overall peak area, consistently lower accumulated chromium on its surface (see Table 1), presents to main deconvolution peaks at 576.7 and 578.5 corresponding to $Cr(OH)_3$ and Cr(VI), respectively (Fig. 5d).

Following the effect of the reversal current on the release of the deposited chromium and regeneration of the membrane and recovering of the water flux, the impact of alternate current (AC) was further evaluated. Based on our previous experience [3], a higher AC potential was applied to achieve similar efficiency of that observed with DC. Thus, Cr(VI) removal was studied at AC potentials of 0.6, 1.0 and 1.5 Vpp (peak-to-peak voltage) at frequencies of 10 Hz and 1 kHz (Fig. 6). The highest efficiency was observed at 1.5 Vpp at 10 Hz. Further increase in frequency from 10 Hz to 1 kHz did not improve the efficiency of the

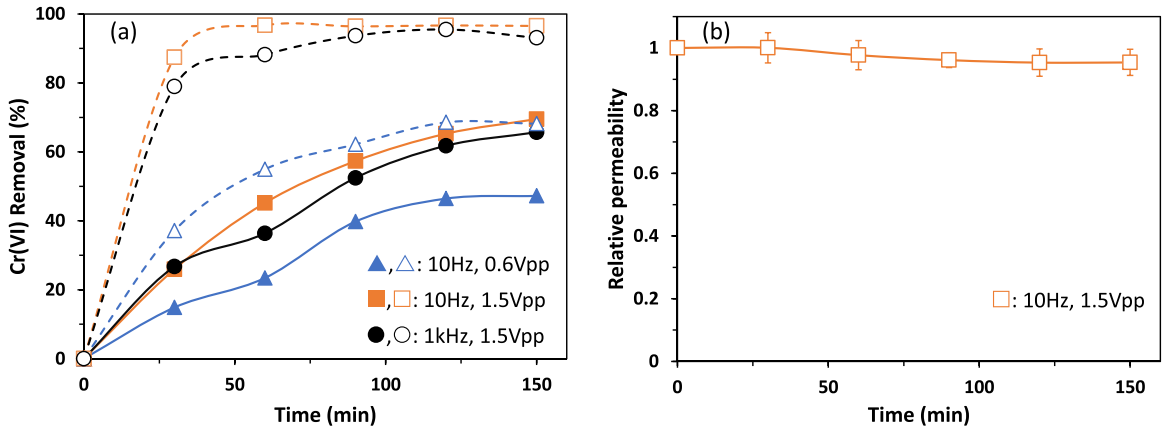

Fig. 6. Hexavalent chromium (2 mg/L) removal in filtration mode in the flow-through electrochemical system with alternate current applied. (a) Removal profile as a function of AC conditions; (b) Relative permeability profile at 1.5 Vpp and 10 Hz. Bulk: solid lines/closed symbols; Membrane: dashed lines/open symbols. AC conditions as indicated. For further details see legend to Fig. 3.

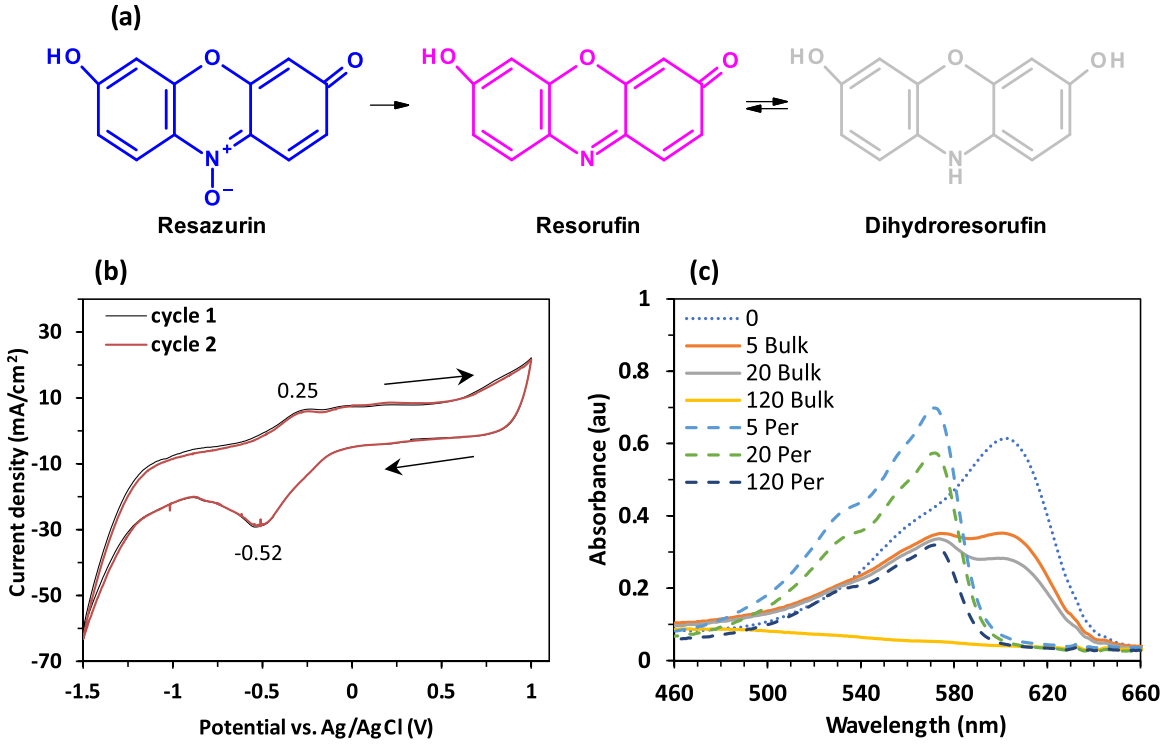

Fig. 7. Resazurin reduction (10 mg/L) in the flow-through electrochemical system with a cathodic CNT membrane and a palladium coated-titanium anode against an Ag/AgCl reference electrode. (a) Scheme of resazurin (blue) reduction to resorufin (pink) and dihydroresorufin (colorless). (b) Cyclic voltammogram of resazurin reduction (2 cycles) at a scan rate of 50 mV/s. (c) Time-profile spectrophotometric scans of resazurin reduction to resorufin at −1 V in filtration mode. Dotted line, time zero (raw feed); solid lines, bulk, comprising the recycled retentate and permeate blended back into the feed; dashed lines, permeate (Per). Numbers in the legend indicate running time in min at which the scan was recorded.

electrochemical system (Fig. 6a). The permeability profile, as shown for the AC potential of 1.5 Vpp and 10 Hz remained relatively steady along the length of the experiment (Fig. 6b), compared to the more pronounced decline in permeability observed under DC cathodic potential (see Fig. 4a). Based on these findings, it can be drawn that AC potential with optimized frequencies would be a good approach for efficient chromium reduction/filtration along with minimization of membrane clogging. However, it needs to be evaluated in more detail in future studies.

3.3. Reduction of resazurin

Next, the proof of concept of the electrochemical system with a CNT cathodic membrane for reduction of organic pollutants was tested first with the reference redox compound, resazurin (7-hydroxy-3 H-phenoxazin-3-one-10-oxide) (Fig. 7). Upon electrochemical reduction, resazurin is irreversibly deoxygenated into resorufin (7-hydroxy-3 H-phenoxazin-3-one), which in turn, and as function of the pH, may be further reversibly reduced to dihydroresorufin (3,7-dihydroxy-phenoxazine) (Fig. 7a). A typical cyclic voltammogram of resazurin reduction in 100 mM Na_2SO_4 electrolyte exhibited a dominant reduction peak at −0.52 V *vs.* Ag/AgCl (Fig. 7b), depicting a typical irreversible reaction

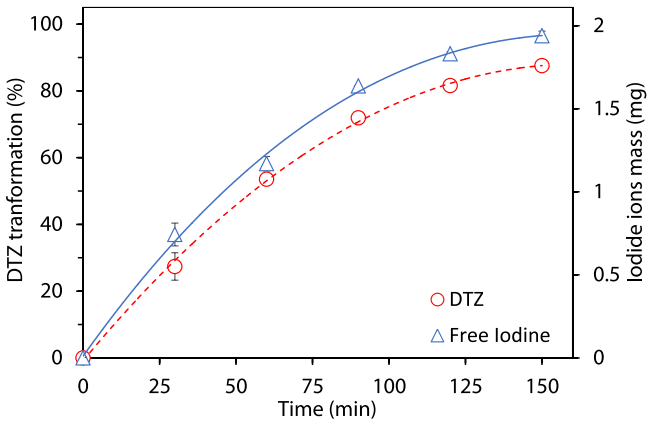

Fig. 8. Removal of diatrizoate in crossflow filtration mode in the electrochemical system at −1 V potential. Transformation indicates the percentage of effective DTZ removal by electrochemical activity measured in the feed tank. Free iodine indicates the total cumulative mass of free iodide ions in the system. Data represent average ± st. dev. The effective initial DTZ concentration was (7.5 ± 0.2 mg/L).

[41]. This dominant reduction peak is related to the transformation of resazurin to resorufin. The reduction of resazurin in the electrochemical system in filtration mode with full recirculation applying −1 V, was tracked by scanning spectrophotometry (Fig. 7c). The blue resazurin (above pH 6.5) turned pink (peak at 605 nm) upon reduction to resorufin (main peak at 570 nm and secondary at 530 nm). The time profile-scans suggest that further partial reduction of resorufin to the colorless dihydroresorufin took place at the pH of the runs, close to neutrality. Resazurin reduction started immediately upon applying an electric potential. Hence, its concentration in the permeate side was null, whereas, in the bulk, gradual transformation and eventually 100% conversion was achieved in 120 min

Comparable results were attained in filtration mode with permeate release and recirculation of the retentate. TOC determination in the bulk and permeate allowed us to confirm that electrochemical reduction was the only pathway responsible for resazurin disappearance, whereas adsorption onto the membrane or mineralization could be neglected (Fig. S2).

Table 2
Transformation products identified during the cathodic reduction of diatrizoic acid in Na_2SO_4 electrolyte.[a]

Nominal molecular mass (Da)	Ion mass in Da, Ion formula, (RT in min.)				Proposed structure of the molecule
	Positive ESI		Negative ESI		
	$[M+H]^+$	$[M+NH_4]^+$	$[M-H]^-$	$[M-H-CO_2]^-$	
TP362	362.98 $C_{11}H_{12}O_4N_2I$ (RT=2.55)	380.01 $C_{11}H_{15}O_4N_3I$ (RT=2.55)	360.97 $C_{11}H_{10}O_4N_2I$ (RT=2.40)		
TP236	237.08 $C_{11}H_{13}O_4N_2$ (RT=3.75)		235.07 $C_{11}H_{11}O_4N_2$ (RT=3.49)		
TP234s	235.07 $C_{12}H_{14}O_3N_2$ (RT=1.52; 2.56; 4.83)				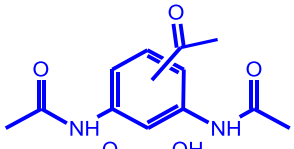
TP252			251.06 $C_{11}H_{11}O_5N_2$ (RT=2.36)		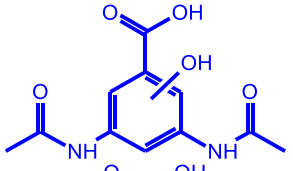
TP307			305.92 $C_9H_9O_3NI$ (RT=4.39)		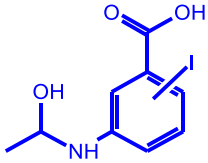
Diatrizoic acid	614.78 $C_{11}H_{10}O_4N_2I_3$ (RT=1.66)	631.80 $C_{11}H_{13}O_4N_3I_3$ (RT=1.66)		568.77 $C_{10}H_8O_2N_2I_3$ (RT=1.53)	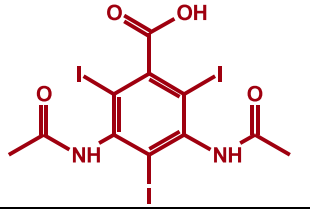

[a] TP: transformation product; RT: retention time.

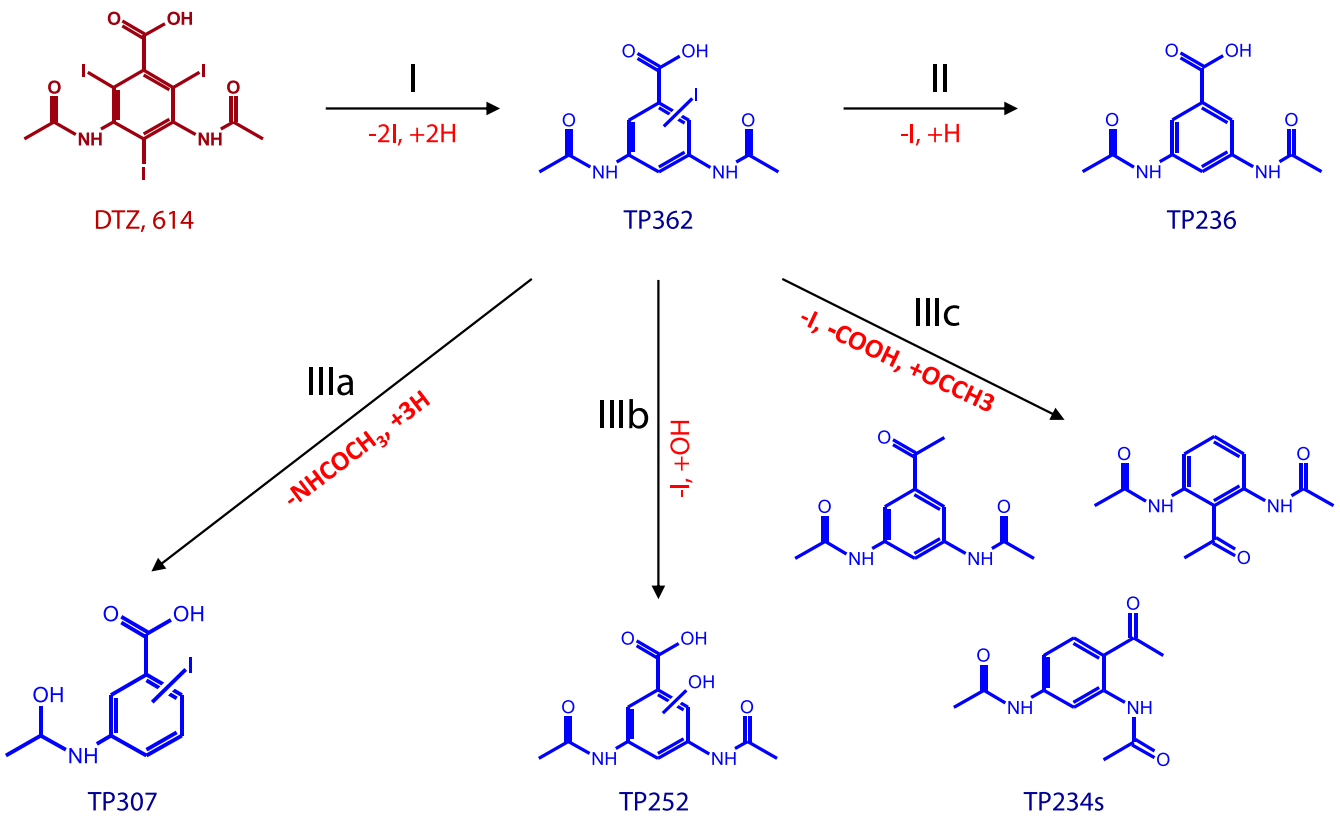

Fig. 9. Proposed transformation pathways for DTZ, in the flow-through electrochemical system with a cathodic CNT membrane and sodium sulfate as electrolyte. I: di-deiodination/reduction; II: deiodination/reduction; IIIa: tautomerization/reduction; IIIb: deiodination/substitution; IIIc: deiodination/decarboxylation/acylation.

3.4. Reduction of diatrizoate

Next, the efficiency of the electrochemical reduction of the halogenated model compound DTZ, was studied. A typical cyclic voltammogram of DTZ reduction in 0.05 M Na_2SO_4 electrolyte exhibited one cathodic peak at −0.35 V and one anodic peak at 0.73 V *vs.* Ag/AgCl (Fig. S3). To comparatively evaluate transformation and deiodination during simultaneous reduction and filtration at −1 V, both changes in concentration of DTZ and iodide were tracked, and the results are presented in Fig. 8.

As shown in Fig. 8, approx. 90% DTZ was transformed after 2.5 h reaction at the conditions applied, following first-order kinetics with a rate constant of 0.014 min^{-1}. As can be seen from the mass balance profile at each sampling time, the transformation of DTZ paralleled the formation of iodide, indicating that deiodination was the main pathway of DTZ transformation under the reduction conditions applied. Exposing a 2 mg/L DTZ solution for 24 h to CNT-laminate slices of increasing surface area in the range of 2–10 cm^2 evidenced that DTZ adsorption was negligible, at a slope of 7.5 pg/m^2.h (see Fig. S3). Based on bond energy and redox potential, at the cathodic potential applied, deiodination could be predicted as the most feasibly electrochemical reaction. In fact, the C-I bond displays the lowest bond energy (240 $kJ/mol_{298\ K}$) compared to other bonds within the DTZ molecule, either in the aromatic ring or in the side chains [42]. This is further supported by the potential of polyhalogenated aromatic to undergo reductive dehalogenation under reducing conditions, regardless of the dehalogenation mechanism [43]. Indeed, reductive dehalogenation becomes more thermodynamically favored with the degree of halogenation and the weakness of the C-halogen bond ([44]).

The structural elucidation and reaction pathways of DTZ transformation during electrochemical reduction with a CNT cathodic membrane was performed by LC-MS (Table 2). This analysis was carried out in a high-resolution mass spectra-orbitrap equipped with a heated ESI operated in negative and positive ionization modes. The samples for analysis were taken at the end of the reaction time (150 min). Overall, 5 transformation products (TP) were identified (TP362, TP236, TP234, TP252, TP307) in positive ionization mode, as either or both $[M+H]^+$ or/and $[M+NH_4]^+$, and/or in negative ionization mode ($[M-H]^-$), as indicated in Table 2. The total and extracted ion chromatograms of intermediates obtained by both positive and negative electron spray ionization mode are presented in Fig. S4. The TPs were named based on their molecular mass derived from the *m/z* value. TP234 was identified in three isomeric forms named TP234s. The error between the measured mass of the TPs and the assigned structures was less than 10 mg/L. Only two transformation products, TP362 (3,5-diacetamido-iodobenzoic acid) and TP236 (3,5-diacetamidobenzoic acid) have been reported in the literature as transformation products of DTZ. The proposed structure of the other TPs are new and were elucidated in this work.

Following the analysis data, three degradation pathways for DTZ transformation under reductive conditions are proposed (Fig. 9). The main transformation pathway consists of a two-step reductive deiodination sequence (I, II), as depicted by the *m/z* values of the molecular ions $[M+H]^+$ and $[M-H]^-$, exhibiting a mass difference of $\Delta m/z = 126$ and its multiples (*m/z* 614.78 → *m/z* 362.98 → *m/z* 237.08/235.07). This indeed indicates a reductive-deiodination sequence of DTZ (614 Da) with substitution of iodine (127 Da) by hydrogen, comprising the formation of 3,5-diacetamido-iodobenzoic acid (TP362) by di-deiodination (pathway I), and then of 3,5-diacetamidobenzoic acid (TP236) by mono-deiodination (pathway II). TP236, corresponding to the most prominent peaks eluting at RT of 3.75 min in positive mode ($[M+H]^+$ ion mass of 237.08 Da) and 3.49 min in negative mode ($[M-H]^-$ ion mass of 235.07 Da) (see Table 2), was by far the major TP accumulated (Fig. S4). The exact position of the remaining iodine in the aromatic ring of TP362 could not be determined in this study. Indeed, 3,5-diacetamidobenzoate has been largely reported as the primary transformation product of DTZ by electrochemical reduction [25,45].

Alternatively, TP362 appears as a pivotal intermediate for three other bifurcating transformations (III). In pathway IIIa, TP362 was converted to TP307 (5[(1-hydroxyethyl)amino-iodobenzoic acid) by modification of the side chains, most probably by tautomerization and reduction processes with cleavage of the amide moiety on one chain, and hydride driven-reduction of the carbonyl to hydroxyl on the other chain. Because of the symmetry of the molecule, it was not possible to elucidate in this study in which side chain each transformation took place. In pathway IIIb, the transformation of TP362 most likely proceeded by deiodination, through nucleophilic substitution of iodine by hydroxyl, towards the formation of TP252 (3,5-diacetamido-hydroxybenzoic acid). The exact position of the hydroxyl in the aromatic ring of TP252 could not be determined in this study. Finally, in pathway IIIc, TP362 was probably transformed by combined deiodination and decarboxylation followed by acylation, towards the generation of three isomeric forms of TP234s. The most stable *p*-isomer (N,N′-(5-acetyl-1,3-phenylene)diacetamide), most likely corresponded to the major peak with a $[M+H]^+$ ion mass of 235.05 Da, eluting at an RT of 2.56 min (see Table 2). Although TP362 is more prone to transformation, the possibility that TP324s may also be formed, at least partially, by successive decarboxylation and acylation of the main product of DTZ transformation, TP236, cannot be ruled out.

4. Conclusions

Highly conductive porous CNT membranes could be used as cathode for electrochemical removal of emerging contaminants from water. This approach, comprising concomitant transformation and separation of dissolved contaminants in crossflow filtration, has the capability to reduce the toxicity of organic and inorganic contaminants at low voltage currents. Indeed, voltages −0.6 to −1.0 V were enough to remove between 90% and 95% of the three model contaminants tested. The removal of hexavalent chromium proceeded by reduction to Cr(III) followed by adsorption onto the cathode. By employing reversal (anodic) potential the membrane could be efficiently regenerated (up to 95%). Preliminary findings applying AC current suggest that it could be a feasible approach for efficient chromium detoxification with minimization of membrane clogging. Resazurin was immediately transformed into resorufin to near completion which was in turn partially reduced to dihydroresorufin. The reductive transformation of diatrizoate resulted in almost complete deiodination, most likely due to the relative lower C-I bond energy, leading to accumulation of 3,5-diacetamidobenzoic acid as the main end-product. Although other five transformation products were detected, four of them were fully deiodinated, indicating that electrochemical reduction/filtration might be an effective mean for detoxification of highly halogenated organic compounds. Concluding, the proposed electrochemical filtration cell equipped with a highly conductive CNT-cathodic membrane can be regarded as a potential technique for wastewater decontamination and effective dehalogenation of organic compounds. Whereas dehalogenation itself reduces toxicity dramatically, post-oxidation treatment might be required for further mineralization of the dehalogenated organic contaminants in some practical applications.

Author contributions

C. Thamaraiselvan: Draft preparation, Writing & editing, Investigation, Methodology, Data curation. W.J Lau: Writing & commenting. C.G. Dosoretz: Conceptualization, Guidance, Resources, Data elaboration, Writing, reviewing & editing.

Declaration of Competing Interest

The authors declare that they have no known competing financial interests or personal relationships that could have appeared to influence the work reported in this paper.

Acknowledgments

This work was funded in part by the Technion-Guangdong fellowship, Israel. The Russell Berrie Nanotechnology Institute (RBNI) at Technion, Israel is gratefully acknowledged for its support. The authors gratefully acknowledge Dr. Yuri Gendel for the technical discussion and lab facilities.

Appendix A. Supplementary material

Supplementary data associated with this article can be found in the online version at doi:10.1016/j.jece.2022.107670.

References

[1] F.C. Moreira, R.A.R. Boaventura, E. Brillas, V.J.P. Vilar, Electrochemical advanced oxidation processes: a review on their application to synthetic and real wastewaters, Appl. Catal. B Environ. 202 (2017) 217–261, https://doi.org/10.1016/j.apcatb.2016.08.037.
[2] Ihsanullah, Carbon nanotube membranes for water purification: developments, challenges, and prospects for the future, Sep. Purif. Technol. 209 (2019) 307–337, https://doi.org/10.1016/j.seppur.2018.07.043.
[3] C. Thamaraiselvan, A. Ronen, S. Lerman, M. Balaish, Y. Ein-Eli, C.G. Dosoretz, Low voltage electric potential as a driving force to hinder biofouling in self-supporting carbon nanotube membranes, Water Res. 129 (2018) 143–153, https://doi.org/10.1016/J.WATRES.2017.11.004.
[4] A. Ronen, S.L. Walker, D. Jassby, Electroconductive and electroresponsive membranes for water treatment, Rev. Chem. Eng. 32 (2016) 533–550, https://doi.org/10.1515/revce-2015-0060.
[5] A. Ronen, W. Duan, I. Wheeldon, S. Walker, D. Jassby, Microbial attachment inhibition through low-voltage electrochemical reactions on electrically conducting membranes, Environ. Sci. Technol. 49 (2015) 12741–12750, https://doi.org/10.1021/acs.est.5b01281.
[6] Y. Yan, J. Miao, Z. Yang, F.-X. Xiao, B.H. Yang, B. Liu, Y. Yang, Carbon nanotube catalysts: recent advances in synthesis, characterization and applications, Chem. Soc. Rev. 44 (2015) 3295–3346, https://doi.org/10.1039/C4CS00492B.
[7] C.D. Vecitis, G. Gao, H. Liu, Electrochemical carbon nanotube filter for adsorption, desorption, and oxidation of aqueous dyes and anions, J. Phys. Chem. C 115 (2011) 3621–3629, https://doi.org/10.1021/jp111844j.
[8] H.-J. Lee, N. Zhang, M.A. Ganzoury, Y. Wu, C.-F. de Lannoy, Simultaneous dechlorination and advanced oxidation using electrically conductive carbon nanotube membranes, ACS Appl. Mater. Interfaces 13 (2021) 34084–34092, https://doi.org/10.1021/acsami.1c06137.
[9] M.S. Rahaman, C.D. Vecitis, M. Elimelech, Electrochemical carbon-nanotube filter performance toward virus removal and inactivation in the presence of natural organic matter, Environ. Sci. Technol. 46 (2012) 1556–1564, https://doi.org/10.1021/es203607d.
[10] C.-Y. Ma, S.-C. Huang, P.-H. Chou, W. Den, C.-H. Hou, Application of a multiwalled carbon nanotube-chitosan composite as an electrode in the electrosorption process for water purification, Chemosphere 146 (2016) 113–120, https://doi.org/10.1016/J.CHEMOSPHERE.2015.12.012.
[11] Y. Liu, J. Yan, D. Yuan, Q. Li, X. Wu, The study of lead removal from aqueous solution using an electrochemical method with a stainless steel net electrode coated with single wall carbon nanotubes, Chem. Eng. J. 218 (2013) 81–88, https://doi.org/10.1016/J.CEJ.2012.12.020.
[12] Y.-X. Liu, D.-X. Yuan, J.-M. Yan, Q.-L. Li, T. Ouyang, Electrochemical removal of chromium from aqueous solutions using electrodes of stainless steel nets coated with single wall carbon nanotubes, J. Hazard. Mater. 186 (2011) 473–480, https://doi.org/10.1016/J.JHAZMAT.2010.11.025.
[13] Y. Zhang, Z. Chen, L. Zhou, P. Wu, Y. Zhao, Y. Lai, F. Wang, S. Li, Efficient electrochemical degradation of tetrabromobisphenol A using MnO2/MWCNT composites modified Ni foam as cathode: kinetic analysis, mechanism and degradation pathway, J. Hazard. Mater. 369 (2019) 770–779, https://doi.org/10.1016/J.JHAZMAT.2019.01.077.
[14] M. Ferreira, M.F. Pinto, I.C. Neves, A.M. Fonseca, O.S.G.P. Soares, J.J.M. Órfão, M. F.R. Pereira, J.L. Figueiredo, P. Parpot, Electrochemical oxidation of aniline at mono and bimetallic electrocatalysts supported on carbon nanotubes, Chem. Eng. J. 260 (2015) 309–315, https://doi.org/10.1016/J.CEJ.2014.08.005.
[15] S.N. Misal, M.-H. Lin, S. Mehraeen, B.P. Chaplin, Modeling electrochemical oxidation and reduction of sulfamethoxazole using electrocatalytic reactive electrochemical membranes, J. Hazard. Mater. 384 (2020), 121420, https://doi.org/10.1016/j.jhazmat.2019.121420.
[16] J.E. Yanez H, Z. Wang, S. Lege, M. Obst, S. Roehler, C.J. Burkhardt, C. Zwiener, Application and characterization of electroactive membranes based on carbon nanotubes and zerovalent iron nanoparticles, Water Res. 108 (2017) 78–85, https://doi.org/10.1016/j.watres.2016.10.055.
[17] A.J. Sutherland, M.-X. Ruiz-Caldas, C.-F. de Lannoy, Electro-catalytic microfiltration membranes electrochemically degrade azo dyes in solution, J. Membr. Sci. 611 (2020), 118335, https://doi.org/10.1016/j.memsci.2020.118335.
[18] L. Zhao, X. Zhang, Z. Liu, C. Deng, H. Xu, Y. Wang, M. Zhu, Carbon nanotube-based electrocatalytic filtration membrane for continuous degradation of flow-through

Bisphenol A, Sep. Purif. Technol. 265 (2021), 118503, https://doi.org/10.1016/j.seppur.2021.118503.
[19] L. Xu, J. Niu, H. Xie, X. Ma, Y. Zhu, J. Crittenden, Effective degradation of aqueous carbamazepine on a novel blue-colored TiO2 nanotube arrays membrane filter anode, J. Hazard. Mater. 402 (2021), 123530, https://doi.org/10.1016/j.jhazmat.2020.123530.
[20] X. Qian, L. Xu, Y. Zhu, H. Yu, J. Niu, Removal of aqueous triclosan using TiO2 nanotube arrays reactive membrane by sequential adsorption and electrochemical degradation, Chem. Eng. J. 420 (Part 2) (2021), 127615, https://doi.org/10.1016/j.cej.2020.127615.
[21] C. Thamaraiselvan, S. Lerman, K. Weinfeld-Cohen, C.G. Dosoretz, Characterization of a support-free carbon nanotube-microporous membrane for water and wastewater filtration, Sep. Purif. Technol. 202 (2018) 1–8, https://doi.org/10.1016/j.seppur.2018.03.038.
[22] S. Çakir, E. Arslan, Voltammetry of resazurin at a mercury electrode, Chem. Pap. 64 (2010) 386–394, https://doi.org/10.2478/s11696-010-0007-9.
[23] S. Khazalpour, D. Nematollahi, Electrochemical study of Alamar Blue (resazurin) in aqueous solutions and room-temperature ionic liquid 1-butyl-3-methylimidazolium tetrafluoroborate at a glassy carbon electrode, RSC Adv. 4 (2014) 8431–8438, https://doi.org/10.1039/C3RA45800H.
[24] A. Sengar, A. Vijayanandan, Comprehensive review on iodinated X-ray contrast media: complete fate, occurrence, and formation of disinfection byproducts, Sci. Total Environ. 769 (2021), 144846, https://doi.org/10.1016/j.scitotenv.2020.144846.
[25] J. Radjenovic, V. Flexer, B.C. Donose, D.L. Sedlak, J. Keller, Removal of the X-ray contrast media diatrizoate by electrochemical reduction and oxidation, Environ. Sci. Technol. 47 (2013) 13686–13694, https://doi.org/10.1021/es403410p.
[26] Y. Mu, J. Radjenovic, J. Shen, R.A. Rozendal, K. Rabaey, Jr Keller, Dehalogenation of iodinated X-ray contrast media in a bioelectrochemical system, Environ. Sci. Technol. 45 (2011) 782–788, https://doi.org/10.1021/es1022812.
[27] E.T. Martin, C.M. McGuire, M.S. Mubarak, D.G. Peters, Electroreductive remediation of halogenated environmental pollutants, Chem. Rev. 116 (2016) 15198–15234, https://doi.org/10.1021/acs.chemrev.6b00531.
[28] S.P. Azerrad, C. Lütke Eversloh, M. Gilboa, M. Schulz, T. Ternes, C.G. Dosoretz, Identification of transformation products during advanced oxidation of diatrizoate: Effect of water matrix and oxidation process, Water Res. 103 (2016) 424–434, https://doi.org/10.1016/j.watres.2016.07.066.
[29] S.P. Azerrad, M. Isaacs, C.G. Dosoretz, Integrated treatment of reverse osmosis brines coupling electrocoagulation with advanced oxidation processes, Chem. Eng. J. 356 (2019) 771–780, https://doi.org/10.1016/j.cej.2018.09.068.
[30] W. Duan, G. Chen, C. Chen, R. Sanghvi, A. Iddya, S. Walker, H. Liu, A. Ronen, D. Jassby, Electrochemical removal of hexavalent chromium using electrically conducting carbon nanotube/polymer composite ultrafiltration membranes, J. Membr. Sci. 531 (2017) 160–171, https://doi.org/10.1016/j.memsci.2017.02.050.
[31] J. Wang, K. Ashley, E.R. Kennedy, C. Neumeister, Determination of hexavalent chromium in industrial hygiene samples using ultrasonic extraction and flow injection analysis, Analyst 122 (1997) 1307–1312, https://doi.org/10.1039/a704474g.
[32] Z. Sun, Z. Liu, B. Han, Y. Wang, J. Du, Z. Xie, G. Han, Fabrication of ruthenium-carbon nanotube nanocomposites in supercritical water, Adv. Mater. 17 (2005) 928–932, https://doi.org/10.1002/adma.200400839.
[33] C.M. Welch, O. Nekrassova, R.G. Compton, Reduction of hexavalent chromium at solid electrodes in acidic media: reaction mechanism and analytical applications, Talanta 65 (2005) 74–80, https://doi.org/10.1016/j.talanta.2004.05.017.
[34] H. Peng, J. Guo, Removal of chromium from wastewater by membrane filtration, chemical precipitation, ion exchange, adsorption electrocoagulation, electrochemical reduction, electrodialysis, electrodeionization, photocatalysis and nanotechnology: a review, Environ. Chem. Lett. 18 (2020) 2055–2068, https://doi.org/10.1007/s10311-020-01058-x.
[35] J. Krejci, Z. Sajdlova, J. Krejci, T. Marvanek, Voltammetry under a controlled temperature gradient, Sensors 10 (2010) 6821–6835, https://doi.org/10.3390/s100706821.
[36] A.J. Bard, L.R. Faulkner. Electrochemical Methods: Fundamentals and Applications, second ed., Wiley, New York, NY, 2001. ISBN: 978-0-471-04372-0.
[37] W. Jin, H. Du, S. Zheng, Y. Zhang, Electrochemical processes for the environmental remediation of toxic Cr(VI): a review, Electrochim. Acta 191 (2016) 1044–1055, https://doi.org/10.1016/J.ELECTACTA.2016.01.130.
[38] C. Thamaraiselvan, A.K. Thakur, A. Gupta, C.J. Arnusch, Electrochemical removal of organic and inorganic pollutants usingrobust laser-induced graphene membranes, ACS Appl. Mater. Interfaces 13 (2021) 1452–1462, https://doi.org/10.1021/acsami.0c18358.
[39] H. Wang, C. Na, Binder-free carbon nanotube electrode for electrochemical removal of chromium, ACS Appl. Mater. Interfaces 6 (2014) 20309–20316, https://doi.org/10.1021/am505838r.
[40] F. Yao, M. Jia, Q. Yang, K. Luo, F. Chen, Y. Zhong, L. He, Z. Pi, K. Hou, D. Wang, X. Li, Electrochemical Cr(VI) removal from aqueous media using titanium as anode: Simultaneous indirect electrochemical reduction of Cr(VI) and in-situ precipitation of Cr(III), Chemosphere 260 (2020), 127537, https://doi.org/10.1016/j.chemosphere.2020.127537.
[41] T. Doneux, L. Bouffier, B. Goudeau, S. Arbault, Coupling electrochemistry with fluorescence confocal microscopy to investigate electrochemical reactivity: a case study with the resazurin-resorufin fluorogenic couple, Anal. Chem. 88 (2016) 6292–6300, https://doi.org/10.1021/acs.analchem.6b00477.
[42] LibreTexts Libraries, Bond Energies, 22 August 2020. ⟨https://chem.libretexts.org/@go/page/1981⟩.
[43] G. Jiang, K. Wang, J. Li, W. Fu, Z. Zhang, G. Johnson, X. Lv, Y. Zhang, S. Zhang, F. Dong, Electrocatalytic hydrodechlorination of 2,4-dichlorophenol over palladium nanoparticles and its pH-mediated tug-of-war with hydrogen evolution, Chem. Eng. J. 348 (2018) 26–34, https://doi.org/10.1016/j.cej.2018.04.173.
[44] C. Lei, F. Liang, J. Li, W. Chen, B. Huan, Electrochemical reductive dechlorination of chlorinated volatile organic compounds (Cl-VOCs): effects of molecular structure on the dehalogenation reactivity and mechanisms, Chem. Eng. J. 358 (2019) 1054–1064, https://doi.org/10.1016/j.cej.2018.10.105.
[45] W. Zhang, I. Soutrel, A. Amrane, F. Fourcade, F. Geneste, Electrochemical processes coupled to a biological treatment for the removal of iodinated X-ray contrast media compounds, Front. Chem. 8 (2020) 646, https://doi.org/10.3389/fchem.2020.00646.